Exploring Magneto-Hydrodynamic Influence on Mixed Convection within a Vented Enclosure Containing a Heat-Conductive Square Column

Zainab K. Radhi, Sana J. Yaseen, Ahmad A. Alsahlani, and Raheem Al-Sabur*

Mechanical Engineering Department, University of Basrah, Basrah, Iraq
Email: zainab.radhi@uobasrah.edu.iq (Z.K.R.); sana.yaseen@uobasrah.edu.iq (S.J.Y.); ahmad.mahdi@uobasrah.edu.iq (A.A.A.); raheem.musawel@uobasrah.edu.iq (R.A.S.)
*Corresponding author

***Abstract*—Heat transfer through mixed convection in obstructed cavities is essential in engineering applications. Magneto-Hydrodynamics (MHD) deals with electrically conductive fluids in a magnetic field. The vented cavities are receiving increasing interest in Convection Heat Transfer (CHT), especially for complex flow patterns and MHD interactions. This study considered a Vented Square Cavity (VSC) and a two-heat-conducting horizontal solid square cylinder. The effect of MHD on mixed convection flow was numerically investigated using FlexPDE software. The study did not focus on specific values of parameters. Instead, it tested a wide range, such as the Hartmann number (Ha) of 10–30, the thermal conductivity solid/fluid ratio of 5–50, the Reynolds number (Re) of 100–500, and the Richardson number (Ri) of 0-10. A wide range of outcomes, including streamlines, isotherms, the average fluid temperature within the enclosure and average Nusselt Numbers (Nu) reflecting heat transfer rates, are exhibited under various parameter settings. It is found that the Ha, Re, and Ri have considerable effects on the flow structure and temperature field. Still, the solid-fluid thermal conductivity ratio has an insignificant impact on the flow field. The results also indicate that the average Nu at the heated wall and the average temperature within the fluid domain are more significant for the considered parameter ranges.**

***Keywords*—Computational Fluid Dynamics (CFD), square column heat transfer, mixed convection, magnetohydrodynamics, MHD modeling, vented cavity, solid block conductivity**

I. Introduction

In the context of studies of heat transfer and fluid dynamics, cavities with obstacles represent any spaces that include solid or porous materials that can hinder the movement of heat transfer or the flow of fluids in the cavities [1]. In engineering applications, notably ventilation of buildings, electronic devices cooling, design of heat exchangers, and heat transfer through mixed convection in obstructed cavities is of great importance [2]. Therefore, understanding such cavities' heat transfer and fluid flow characteristics is imperative to enhance thermal performance and efficiency [3]. Many tools have been developed to solve complex phenomena in heat transfer and fluid flow, where Computational Fluid Dynamics (CFD) has become one of the most essential tools in recent years [4].

Magneto-Hydrodynamics (MHD) deals with electrically conductive fluids in a magnetic field. Such interesting phenomena have made MHD an essential area for research in engineering applications, especially concerning performance enhancement [5]. For example, MHD applications are found in power generation [6], space propulsion [7], nuclear engineering [8], electromagnetic pumps and stirrers [9], geophysics [10], and astronomy [11]. MHD studies on Convection Heat Transfer (CHT) in cavities, such as square, rectangular [12], and triangular cavities with radiation effect [13], triangular cavities with condition effect [14], triangular cavities with Joule heating effect [15] and sometimes extended to specific shapes such as (Shape 'L') [16] and sinusoidal corrugated cavities [17], varied widely. This study focuses on exploring MHD's effects on mixed convection within the Vented Square Cavity (VSC).

Vented square cavities are receiving increasing interest in CHT for several reasons, the most important of which is their relevance to the real world through many applications, including complex flow patterns and MHD interactions, which generally enhance heat transfer.

In this study, FlexPDE will simulate fluid flow and heat transfer behaviour by focusing on changes in the *Ri* and *Re* numbers solid-fluid thermal conductivity *K* and the effects of changing magnetic fields. Subsequent sections will provide an essential summary of the geometry of the problem and the various techniques used, along with a review of the equations used.

II. Literature Review

A comprehensive literature review was conducted to comprehend the existing task of mixed CHT in cavities,

Manuscript received August 21, 2023; revised September 11, 2023; accepted October 16, 2023; published January 29, 2024.

especially when obstacles are presented. A noteworthy study by Rahman *et al.* [18] used a heat-conducting horizontal solid circular cylinder positioned at the cavity's center. They emphasized that the pivotal factor significantly influencing fluid dynamics and heat transfer performance in steady mixed convection scenarios is the Ri number, and they also found that the diameter of the cylinder is part of the effect on the VSC. Alam [19] concluded that increasing magnetic field intensity leads to the suppression of heat transfer. At the same time, increasing nanoparticle volume fraction and Richardson number improves heat transfer through a numerical study of mixed convection in a square enclosure in the presence of an external magnetic field. Hassen *et al.* [20] investigated that enhanced heat transfer was observed with increased magnetic field inclination, more excellent permeability, and higher cylinder speeds during the study of mixed convection and entropy generation in a partitioned porous cavity with dual inner rotating cylinders under the impact of a magnetic field. Furthermore, the study demonstrated complex multicellular flow patterns resulting from the interplay of natural convection, wall motion, and cylinder rotation.

Ali *et al.* [21, 22] also dealt in two studies with a nanofluid subjected to a magnetic field through mixed convection flow in a tubular enclosure. They gave precise parametric discussions for temperature and flow distributions regarding average heat transfer rate, isotherms, and streamlines within the flow domain. Within a comprehensive numerical investigation, Rahman *et al.* [23] investigated MHD during mixed convection resulting from a lid-driven cavity containing a horizontal cylinder inside. They found that the thermal conductivity of the cylinder has a significant effect on the distribution of isotherms within the system and that this effect far exceeds the effect of other parameters. Tang and Li [24] examined mixed convection within a vertical square cavity with lid-driven, differentially heated walls and four hot cylinders in a diamond pattern. They assessed various parameters, including wall motion direction, cylinder spacing, and the *Ri* number. Conclusions revealed optimal heat transfer efficiency at specific Ri numbers and sensitivities to wall motion direction. Ahammed *et al.* [25] investigated the influence of the obstacle diameter and the solid-fluid thermal conductivity ratio on a VSC's flow and thermal fields. They found that decreasing the thermal conductivity ratio and block size can magnify the heat transfer phenomenon. Rais *et al.* [26] investigated mixed convection heat transfer in a lid-driven square enclosure with an isothermal, clockwise rotating cylinder at its centre. The study concealed a range of Re (31.623 to 316.23), Gr (10^3 to 10^5), Ri (0.1 to 10), and internal heat generation coefficients (10, 0, −10) to examine the average Nu number and average drag coefficient on the sliding lid. Ali *et al.* [27] used a rotating cylinder and horizontal baffles to numerically study the changes in mixed CHT in a nanofluid-filled lid-driven square. They confirmed that the roughness of the cylinder, its rotational speed, the lengths of the baffles, and the Hartmann number influence heat transfer and the flow field. Mahmood [28] analysed natural convection from a horizontal cylinder in a square enclosure with water and air as heat transfer fluids and investigated surface temperatures: 303 K to 414 K. Used 2D CFD, comparing Nu to experiments (max error 13%). Their findings were the significant impact of surface temperature on Nu when surrounded by air (0.007 m/s to 0.11 m/s) and dominance of conduction when in water (0.3 m/s at 350 K). Another research team [29] used a pair of rotating cylinders and an inclined magnetic field, and their investigations showed that the inclined magnetic field and wavy surfaces have a direct effect in addition to the effect of the speed of the rotating cylinders on the heat transfer mechanism. On the other hand, good ventilation is considered in a numerical study of the effect of heat transfer by mixed convection when applying a magnetic field in a VSC filled with water. As in many previous studies, the effect of the Ha number was of great importance in decreasing the heat transfer rate [30].

Although many previous studies, especially those reviewed above, have provided valuable insights into magneto-hydrodynamic effects on mixed convection, numerous research aspects still require further investigation. This study endeavors to bridge these research gaps by conducting a comprehensive parametric analysis of magneto-hydrodynamic impacts on mixed convection within a Vented Square Cavity (VSC). The study investigation encloses a wide parameter range, including the influence of material properties, complex flow patterns, streamlines, and the variation of Nusselt numbers. Besides, the study comprises the sight of heat-conducting two-square cylinder obstacles, introducing specific geometric complexities to ensure a thorough exploration of this multifaceted phenomenon.

III. Materials and Methods

A. Physical Model Geometry

Exploration of the effects of MHD on heat transfer and fluid flow is a significant factor in this investigation. As shown in Fig. 1, an essential aspect of the study is concentrated in the left part, specifically in the lower corner. A square (L) Length (cavity) container was used. Inside the container are two cylindrical structures with length (Lx) and thermal conductivity (Ks). As limiting conditions in this investigation, a uniform constant temperature (Th) was considered for the right side, while an adiabatic condition was adopted for the rest of the surfaces. Then, two holes served as openings in the container used for fluid flow; the first was centered at the bottom of the left vertical wall, while the other was at the top of the opposite (hot) wall. The two openings were equal and measured (W = 0.1L). In addition, a constant magnetic field (Bo) was applied horizontally on the hot wall to study the effect of the magnetic field. The air velocity is assumed to be constant (ui), and the ambient temperature is (Ti). Adopt zero diffusion flux for all variables for outgoing flow depending on convective boundary conditions. Concerning solid boundaries of the VSC, it was considered rigid non-slip walls, which means the fluid velocity at the walls is zero.

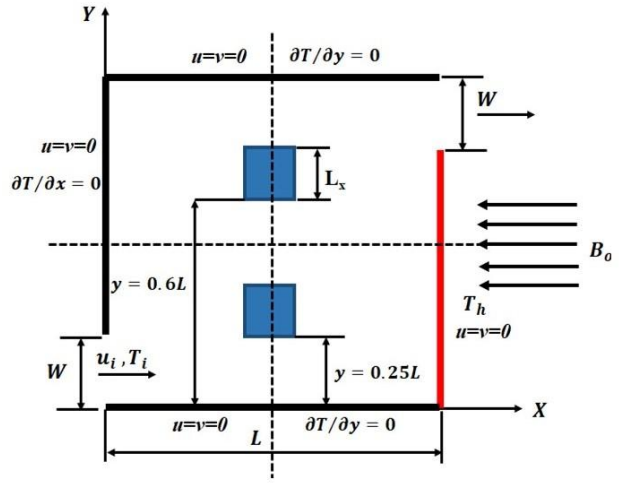

Fig. 1. Schematic of the physical model.

B. Methodology

The energy, continuity, and momentum equations as non-dimensional forms defining the flow under the usual Boussinesq assumption are as follows [31]:

$$U\frac{\partial\theta}{\partial X}+V\frac{\partial\theta}{\partial Y}=\frac{1}{Re\,Pr}\left(\frac{\partial^2\theta}{\partial X^2}+\frac{\partial^2\theta}{\partial Y^2}\right) \quad (1)$$

$$\frac{\partial U}{\partial X}+\frac{\partial V}{\partial Y}=0 \quad (2)$$

$$U\frac{\partial U}{\partial X}+V\frac{\partial U}{\partial Y}=-\frac{\partial P}{\partial X}+\frac{1}{Re}\left(\frac{\partial^2 U}{\partial X^2}+\frac{\partial^2 U}{\partial Y^2}\right) \quad (3)$$

$$U\frac{\partial V}{\partial X}+V\frac{\partial V}{\partial Y}=-\frac{\partial P}{\partial Y}+\frac{1}{Re}\left(\frac{\partial^2 V}{\partial X^2}+\frac{\partial^2 V}{\partial Y^2}\right)+Ri\theta-\frac{Ha^2}{Re}V \quad (4)$$

The equation of energy for the solid cylinder is [18]:

$$\left(\frac{\partial^2\theta_s}{\partial X^2}+\frac{\partial^2\theta_s}{\partial Y^2}\right)\frac{K}{Re\,Pr}=0 \quad (5)$$

The dimensionless variables utilized in the above equations are described as:

$$X=\frac{x}{L},\quad Y=\frac{y}{L},\quad U=\frac{u}{u_i}$$

$$V=\frac{v}{u_i},\quad P=\frac{p}{\rho u_i^2}$$

$$\theta=\frac{T-T_i}{T_h-T_i},\quad \theta_s=\frac{T_s-T_i}{T_h-T_i}$$

The controlling parameters of the governing equations are Re, Ri, Ha, Pr, and solid-fluid thermal K_s are defined as [18]:

$$Re=\frac{u_i L}{v},\quad Ri=\frac{g\beta(T-T_i)L}{u_i^2}$$

$$Pr=\frac{v}{\alpha},\quad and\ K=\frac{k_s}{k}$$

The average Nu on the heated wall and the bulk average temperature in the cavity are defined as:

$$Nu=\frac{1}{L_h}\int_0^{L_h}\frac{\partial\theta}{\partial X}dY,\qquad \theta_{av}=\frac{1}{V}\int\theta d\overline{V}$$

L_h represents the length of the heated wall, and V is the VSC volume.

C. Boundary Conditions

As indicated in Fig. 1, suitable boundary conditions for the above equations as dimensionless forms are U=1, V=0, and θ=0 at the inlet, while the Convection Boundary Condition (CBC) and P=0 at the outlet. At all solid boundaries, U and V are kept equal to zero, and at the left, top, and bottom walls:

$$\left(\frac{\partial\theta}{\partial Y}\right)_{Y=1}=\left(\frac{\partial\theta}{\partial X}\right)_{X=0}=0$$

At the solid-fluid vertical and horizontal interfaces of the cylinder:

$$K\left(\frac{\partial\theta_s}{\partial X}\right)_{solid}=\left(\frac{\partial\theta}{\partial X}\right)_{fluid}$$

$$K\left(\frac{\partial\theta_s}{\partial Y}\right)_{solid}=\left(\frac{\partial\theta}{\partial Y}\right)_{fluid}$$

D. Numerical Technique

The Galerkin weighted residual method is used for the numerical solution. FlexPDE software analyzes the mixed convection in a VSC with a two-heat conduction solid cylinder [32]. As a result of the pressure inclusion in the equations of momentum, many solutions to Eq. (1)–Eq. (5) often involve strong oscillations, and sometimes there is an indeterminate solution. The finite element method uses a derived approach, allowing standard grids and elements to stabilize pressure oscillations. This strategy executes the equation of continuity and the pressure to provide an approach called the penalty strategy [33].

$$\nabla^2 P=\lambda\left(\frac{\partial U}{\partial X}+\frac{\partial V}{\partial Y}\right) \quad (6)$$

The λ values are selected according to the experience or depending on the previous studies. Usually, a λ of 1e5 is used [33], which was chosen for this formulation. So, Eq. (2) can be excluded, and Eq. (6) is used instead.

E. Grid Refinement and Validation

In heat transfer problems that are solved numerically, the grid refinement test is a pivotal aspect in achieving a systematic increase in the accuracy of the computational grid and an effective contribution to the convergence of simulation results. A grid refinement test was conducted for mixed convection in a VSC at respective values of Ha = 10, Ri = 1, Re = 100, and K = 5 to get a grid-independent solution. A 2D simulation of four different triangular meshes was used. Table I shows that the grid encompasses 6,987 nodes and 3,420 elements, ensuring a sufficient level of spatial resolution to represent the base case geometry. A comprehensive analysis was performed to optimize

accuracy and computational efficiency in deciding the grid size for the numerical simulations. Several grid sizes were assessed, including larger grids with 29,011 nodes and 14,314 elements. The final grid selection with 6,987 nodes and 3,420 elements was based on its consistent ability to yield results that closely matched those obtained with the larger grid while significantly decreasing computational time. This approach ensures the numerical simulations are accurate and computationally efficient, allowing for precise results within appropriate computational timeframes. The approach was grid size-independent with additional refinement. Fig. 2 indicates the numerical mesh mode for the current study.

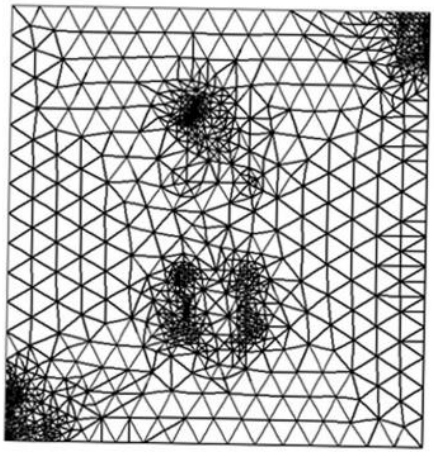

Fig. 2. Schematic diagram of the continuum domain.

TABLE I. SENSITIVITY OF GRID TEST AT HA=10, RE=100, K=5, AND RI=1

Nodes (Elements)	1,353 (638)	1,977 (942)	6,987 (3,420)	29011 (14,314)
Nu	4,652	4,594	4,621	4,628
Θav	0.167	0.173	0.175	0.174
Time(s)	196	706	3,333	19,440

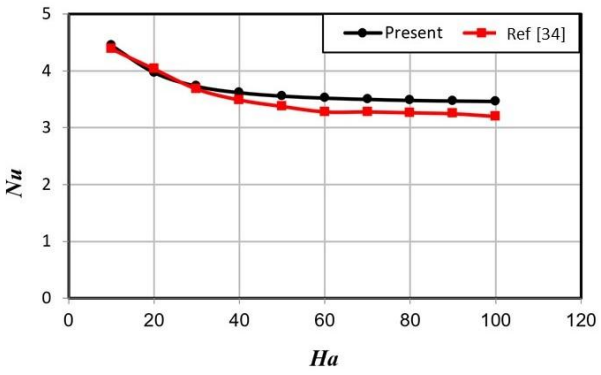

Fig. 3. Comparison between the present study and [34] for the influence of Hartmann number on average Nusselt number in the VSC at Re = 100.

The evaluation and reliability of the results of the current investigation are essential, and comparison with previous studies gives this study more acceptability, so it was compared with [34], which focuses on the mixed magnetic-hydrodynamic heat flow in a VSC. Fig. 3 compares the extent to which the average Nu number is affected by the change in Ha number between the results of this study and the comparative study. The explicit agreement and consistency between the two give the general impression that the numerical approach used in this study is robust and worthy of use.

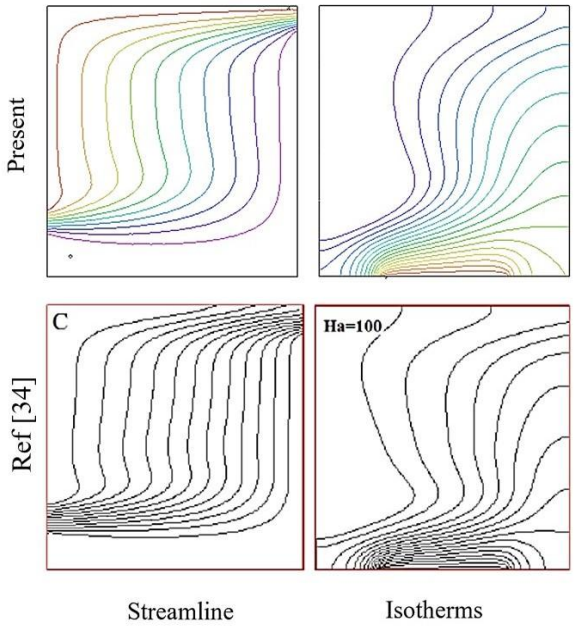

Fig. 4. Validation of isotherms and streamlines at Ha = 100, Ri = 1, and Re = 100.

On the other hand, Fig. 4 includes another comparison between the two studies related to streamlines and isotherms. There was also excellent agreement for heat transfer and flow in specific conditions, noting that the validation was at Ha = 10, Ri = 1.0, Re = 100, and K = 5. These validation cases encourage confidence in the numerical outcome of the current study.

IV. RESULT AND DISCUSSION

The current investigation attempted to explore in depth numerically the 2D heat transfer, in addition to studying the resulting mixed convection from adding two horizontal square cylinders inside the VSC. The research explores the effect of changes in Ha, Ri, and Re numbers on the resulting streamlines and isothermal lines. The investigation was also extended to include the effect of the thermal conductivity ratio between the solid surfaces and the surrounding fluid (air). Prandtl's number of 0.71 was adopted for this study.

The following results provide a clear visualization and an in-depth understanding of the mechanism for distributing isothermal lines and streamlining the cavity. It also systematically describes the average fluid temperature distribution inside the cavity and average Nu at the hot wall, thus giving a comprehensive view of the effect of adding the two square cylinders and shed a magnetic field on the overall system.

A. *Effects of Hartmann Number (Ha)*

The Ha number plays a significant role in MHD flows; when Ha >> 1, the magnetic force dominates over the viscous force, suppressing fluid motion and forming stable layers [35]. A detailed investigation of how the flow and temperature fields are affected by the variation of the Ha number can be found in Figs. 5–6. The results obtained at specific parameters Re = 100, Ri = 1, and K = 5 give more valuable insights into mixed convection's complex Magneto-Hydrodynamics (MHD) when solid square cylinders are present. Initially, at a low value (Ha = 10) as indicated in Fig. 5(a), it is observed that the mainstreams wrap around the two rigid square horizontal cylinders, and it extends almost throughout the VSC. Such behavior can constrain mixing between the inner fluid, which is hot, and the entering colder fresh fluid, creating a stratified flow pattern. This ability of the mainstreams to wrap the cylinders reduces the interaction between incoming and inside fluids and can, therefore, produce distinct thermal patterns.

Higher Ha numbers generally stabilize the fluid flow in heat convection systems implicating conducting fluids and magnetic fields [36]. This stability appears due to the magnetic field's ability to repress the formation of eddies and turbulence. The convection patterns can be varied or suppressed, involving heat transfer elements.

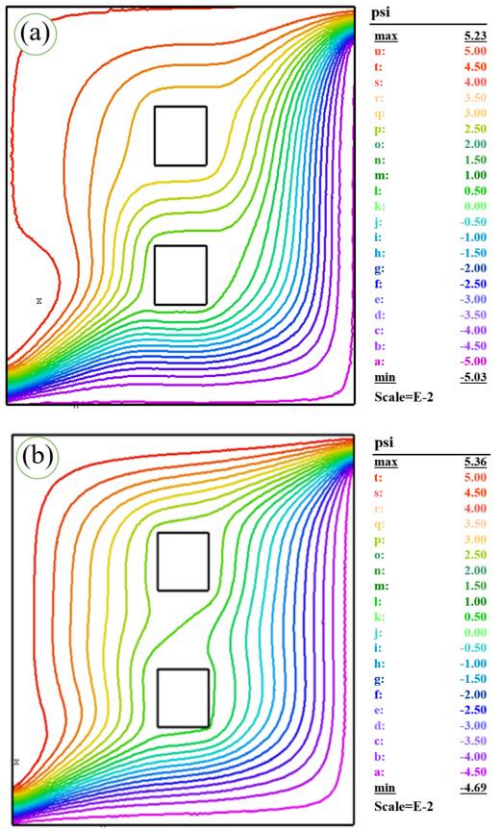

Fig. 5. Streamlines variation according to Hartmann number: a) Ha=10, b) Ha=30 at Re=100, Ri=1 and K=5.

Although the Hartmann number tripled (Ha = 30), the results of the streamlines did not show a noticeable difference and were not affected by the increase in the magnetic field, as shown in Fig. 5(b). The streamlines became closely packed around the two square cylinders inside the VSC due to the suppression of vortex formation in the region as a reflection of the increase in the magnetic field.

Regarding isotherms, as shown in Figure 6a, isotherms appear stratified near the heated surface when the Hartmann number is low (Ha = 10), indicating that there is small diffusion-dominated heat transfer. But when the Hartmann number is tripled to (Ha = 30) in the same way streamlines were studied, isotherms become increasingly deformed from the shapes fitting to diffusion heat transfer, as indicated in Fig. 6(b). This deformation is due to the increase in the effect of the magnetic field on the heat transfer processes and, thus, the irregularity in the temperature distribution inside the VSC.

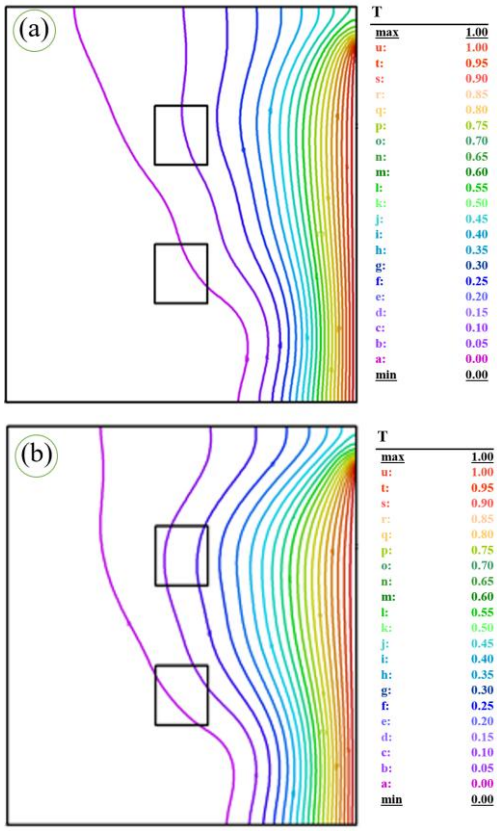

Fig. 6. Isotherms variation according to Hartmann number: a) Ha=10, b) Ha=30 at Ri=1, Re=100, and K=5.

In magnetic fields studies in cavities, it is essential to understand how magnetic fields affect the heat transfer rate along the hot wall so that the changes in the mean Nu number and the mean temperature of the fluid θav are studied according to the shift in Ha number and Ri number. As indicated in Fig. 7, it is observed that Nu increases with the increase of *Ri*. It is always more elevated for the small values of *Ha* (i.e., Ha=10), which refers to more down heat transfer rates for the VSC as the magnetic field strength grows. Regarding the average fluid temperature (θav), as shown in Fig. 8, it can be observed that when the low values of (Ri < 3), there is a convergence in the (θav) values, but here a clear difference appears as the (Ri) increases. At low Ri, the buoyant force has a relatively inefficient impact on the fluid flow. As a result, there is a

convergence in θav values as the effect of buoyancy on fluid velocity and density variations is limited. Regardless, as the Ri grows, the buoyant force evolves more significantly, which leads to a decrease in fluid density and an increase in fluid velocity due to the growth of the thermal boundary layer within the gap. Accordingly, the liquid temperature increases due to improved thermal mixing and heat transfer.

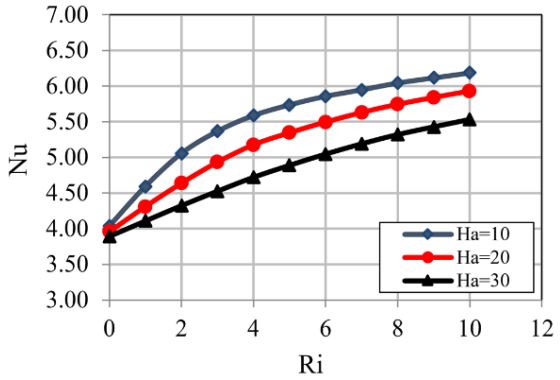

Fig. 7. Influence of Ha on average Nu number at K=5 and Re=100.

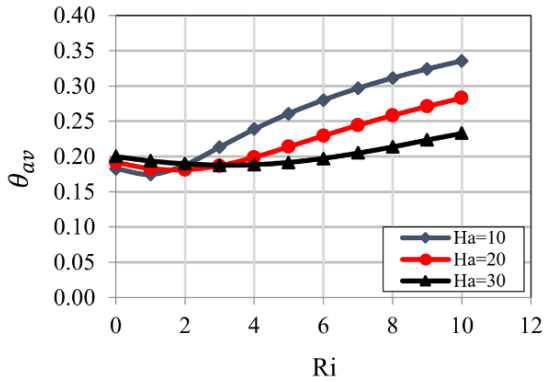

Fig. 8. Influence of Ha on average temperature at K=5 and Re=100.

B. *Effects of Reynolds Number, (Re)*

In fluid dynamics, the Re number is crucial in determining the flow type through its direct effect on inertial and viscous forces within a flowing fluid. The current study explored the expected effects on flow behaviour within the Vented Square Cavity (VSC) under specific Ri = 1, Ha = 10, and K = 5 conditions.

Fig. 9a reviews the behaviour of the streamlines when the Re number is low (Re = 100). The flow path is well-defined, and the streamlines extend from the inlet of the VSC to its exit. The results show that the obstructions led to a coherent pattern of flow.

In contrast, the effects resulting from the increase of the Re number to 500 are shown in Fig. 9b, where it is noted that a shift in the fluid dynamics has occurred. It is also remarkable that the streamlines formed a large circle that covered the entire space inside the VSC, especially around the solid bodies. The resulting behaviour can be explained by the fact that the entrance openings played an essential role in the formation of this complex structure of the flow, which led to a more intense movement.

Moreover, a small vortex was observed near the lower part of the body, resulting from the complex interaction within the VSC due to changes in temperature and pressure. The overall results indicate that the Re number is an influential factor in such types of flow, especially with the presence of magnetic fields.

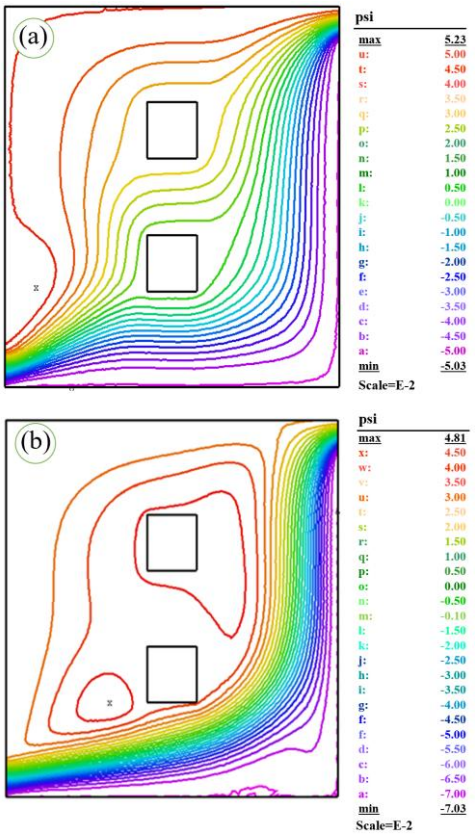

Fig. 9. a) Re=100, b) Re=500 at Ri=1, Ha=10, and K=5; Streamlines variation according to Reynolds number.

Fig. 10a shows the corresponding temperature distribution where the hot wall is characterized by nearly parallel isothermal lines for *Re*=100, similar to conduction-like distribution. At *Re*=500, the Isothermal behavior begins to denser close to the hot wall due to the convective current's strong influence, as shown in Fig. 10b.

The effect of the *Re*, Nu numbers at the hot wall and the average temperature in the enclosure are exhibited as a relation of the *Ri* as in Fig. 11 and Fig. 12, where specific values of *Re* (100, 300, and 500) were selected. It is noted that there is a proportionality that occurs for the Nu number with the increase in the numbers *Ri* and *Re*. The average fluid temperature (θ av) behaviour also does not differ, especially at $1 \leqslant Ri$. The complex interplay between forced convection and buoyancy-driven natural convection effects in the VSC with the heat-conducting square cylinder can significantly impact these changes. As the Richardson Number boosts, it denotes a higher contribution of buoyancy forces than the inertial forces. The Reynolds Number (*Re*) increase also improves the forced convection effect. Higher *Re* values indicate higher fluid speeds within the VSC, increasing convective heat transfer.

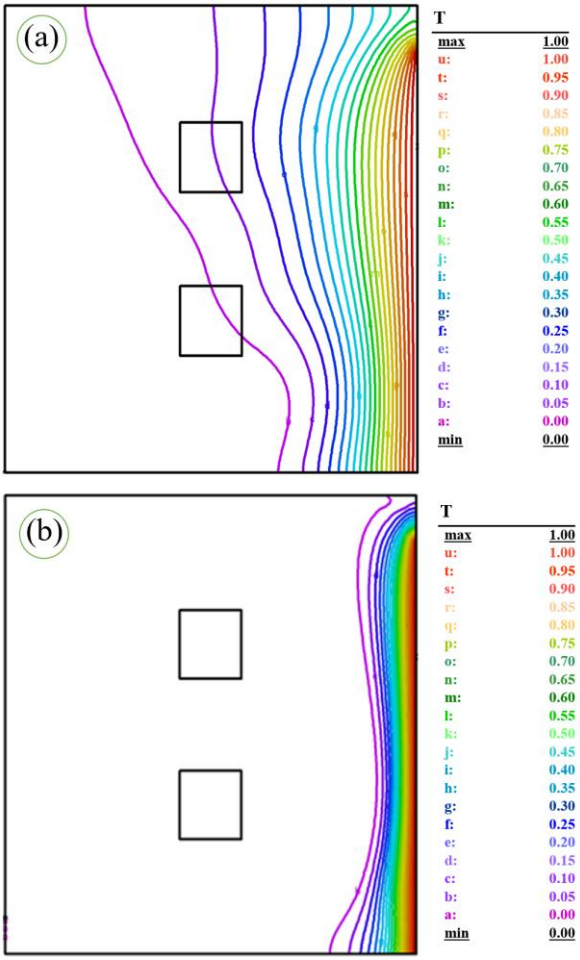

Fig. 10. a) Re=100, b) Re=500 at Ri=1, Ha=10, and K=5; Isothermal lines variation according to Reynolds number.

On the other hand, the increase in the average temperature of the fluid in the VSC because of the increase in the Nu number with the rise in the Ri and Re numbers will lead to convection becoming more diffuse than conductive heat transfer, which means an increase in (θav).

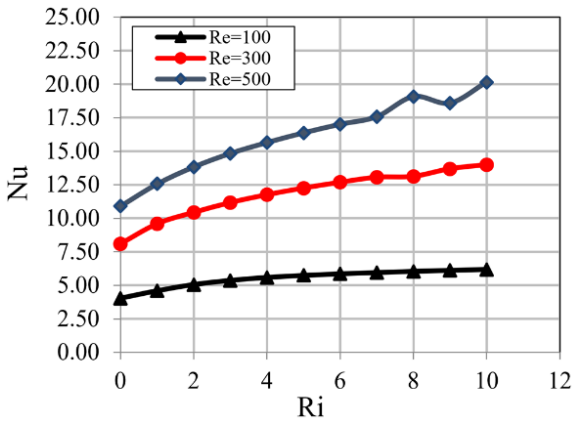

Fig. 11. Influence of Re on average Nu number at K=5 and Ha=10.

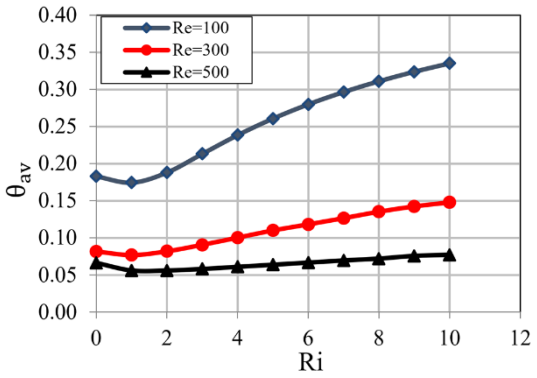

Fig. 12. Influence of Re on average temperature at K=5 and Ha=10.

C. *Effects of Richardson Number, (Ri)*

The streamlines and isotherms design sensitivity concerning the deviation in *Ri* is demonstrated in Figs. 13 –14, respectively, for Ha=10, Re=100, and K=5. When the forced convection is pure at Ri=1, the streamlines are arranged approximately in parallel lines, rounding the two bodies inserted in the cavity and covering the enclosure's surface. However, with the increased Richardson number, Ri=10, the vortex spreads. Furthermore, the generated flow is pressed, and the vortex almost encircles the VSC, demonstrating the natural CHT's dominance. The related isothermal lines in Fig. 12 become nonlinear, forming a plume, indicating the natural CHT's supremacy over conduction and forced convection in the VSC.

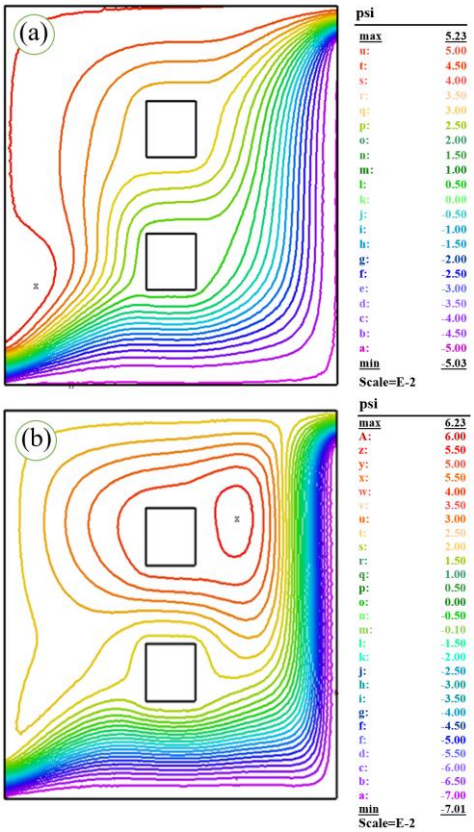

Fig. 13. Streamlines variation according to Richardson number a) Ri=1, b) Ri=10 at Re=100, Ha=10, and K=5.

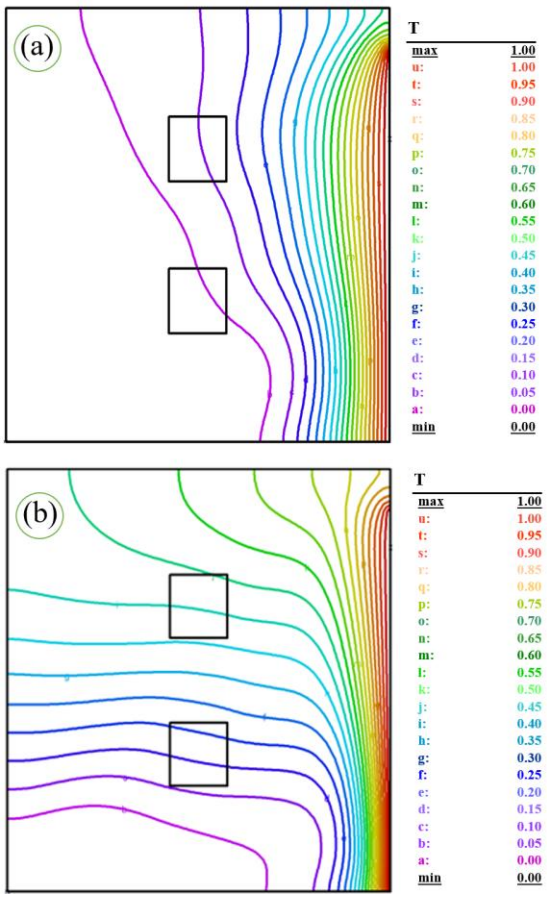

Fig. 14. Isothermal lines variation according to Richardson number a) Ri=1, b) Ri=10 at Re=100, Ha=10, and K=5.

D. *Effects of Thermal Conductivity Ratio, (K)*

The thermal conductivity results on laminar heat transfer and mixed convection flow in a VSC are presented by plotting the Nu number, which enclosure as a function of the Ri number for the three different thermal conductivity. Fig. 15 indicates that the Nu goes up penetratingly with increasing Ri for all values of K. As the Ri grows, the buoyant force becomes more dominant in controlling the fluid's flow patterns and thermal features. At higher Ri values, buoyancy-driven flow induces vigorous fluid motion, increasing turbulence, and enhanced thermal mixing. The result intensifies mixing, guiding to better efficient heat transfer from the heat-conducting square cylinders to the surrounding fluid.

Moreover, the patterns of different thermal conductivity values, K (5,30,50), are fitting together due to the small effect of the thermal conductivity on the heat transfer rates. Fig. 16 illustrates the θ av in the enclosure as a function of the Ri number for three different K. It observed that the θ av has a similar behavior according to the Ri variation for all thermal conductivity ranges, where it is decreased for ($0 \leqslant$ Ri $\leqslant 1$) and growths for ($1 \leqslant$ Ri $\leqslant 10$) due to the increasing of the outcome of the buoyancy with the increasing of Ri which leads to a decrease in the fluid density and an increase in fluid velocity, and thus the fluid temperature increases due to the growth of the thermal boundary layer inside the cavity.

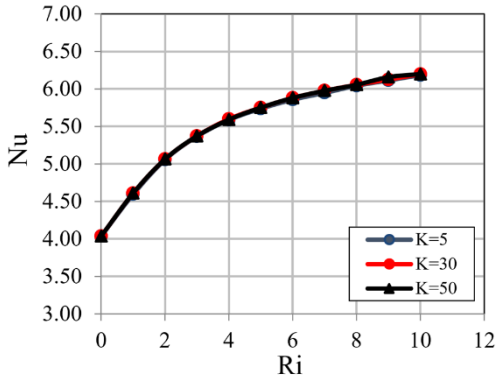

Fig. 15. Influence of K on average Nu number at Ha=10 and Re=100.

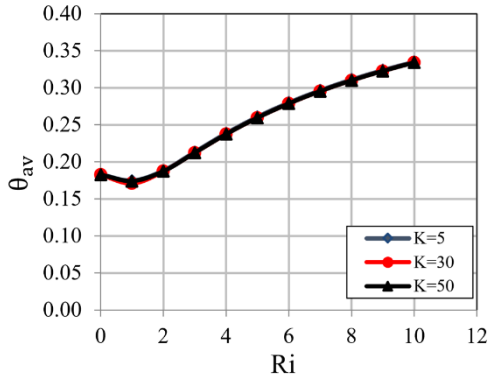

Fig. 16. Influence of K on average temperature at Ha=10 and Re=100.

V. Conclusion

A comprehensive numerical analysis was undertaken to investigate the intricacies of mixed convection within a Vented Square Cavity (VSC), including two square cylinders with heat-conducting abilities. The investigation's coverage contained A comprehensive exploration across various scopes of parameter variations. It spans the solid-fluid thermal conductivity ratio and the Hartmann, Reynolds, and Richardson numbers.

The analysis concluded with accurate, valuable, and exciting results for a greater understanding of the studied phenomena, which the following gains can summarize:

- The heat transfer and the flow characteristics inside the enclosure of the vented square cavities depend strongly upon the magnetic field strength.
- Re-number variation strongly affects the enclosure's streamlines and isotherm structures. Large Re is associated with higher heat transfer rates, while the Re of 500 was associated with the lowest average temperature.
- For all cases, the heat transfer rate increases with the increasing *Ri* number.
- A minimal effect of the thermal conductivity of the solid square bodies' parameters on the streamlines and isotherms is observed.

Nomenclature

Bo: magnetic induction (Wb/m^2)
g: gravitational acceleration (m/s^2)
Gr: Grashof number

h: convection heat transfer coefficient (W/m2K)
Ha: Hartmann number
k: thermal conductivity of fluid (WK/m)
ks: thermal conductivity of solid (WK/m)
K: solid fluid thermal conductivity ratio
L: length of the cavity (m)
Nu: Nusselt number
p: dimensional pressure (N/m^2)
P: dimensionless pressure
Pr: Prandtl number
Re: Reynolds number
Ri: Richardson number
T: dimensional temperature
u, *v*: dimensional velocity components (m/s)
U, *V*: dimensionless velocity components
$\overline{V}$: cavity volume (m^3)
W: height of the opening (m)
x, *y*: Cartesian coordinates (m)
X, *Y*: dimensionless Cartesian coordinates
Greek symbols
α: thermal diffusivity (m^2/s)
β: thermal expansion coefficient (1/K)
υ: kinematic viscosity (m_2/s)
θ: non dimensional temperature
ρ: density of the fluid (kg/m^3)

CONFLICT OF INTEREST

The authors declare no conflict of interest.

AUTHOR CONTRIBUTIONS

S. J. Yaseen provided the conceptual foundation, Z. K. Radhi conducted numerical simulations, A. A. Alsahlani discussed the results, and R. Al-Sabur contributed overall insights and manuscript writing; all authors had approved the final version.

REFERENCES

[1] G. Saha, A. A. Y. A. Waaly, M. C. Paul, and S. C. Saha, "Heat transfer in cavities: Configurative systematic review," *Energies (Basel)*, vol. 16, no. 5, p. 2338, Feb. 2023.

[2] F. Selimefendigil and H. F. Öztop, "Thermal management and performance improvement by using coupled effects of magnetic field and phase change material for hybrid nanoliquid convection through a 3D vented cylindrical cavity," *Int J Heat Mass Transf*, vol. 183, 2022.

[3] W. B. Ye, D. S. Zhu, and N. Wang, "Fluid flow and heat transfer in a latent thermal energy unit with different phase change material (PCM) cavity volume fractions," *Appl Therm Eng.*, vol. 42, pp. 49–57, Sep. 2012.

[4] R. Singh and V. Sharma, "CFD based study of fluid flow and heat transfer effect for novel turning tool configured with internal cooling channel," *J. Manuf Process*, vol. 73, 2022.

[5] W. D. S. Fonseca, R. C. F. Araújo, M. D. O. E. Silva, and D. O. D. A. Cruz, "Analysis of the magnetohydrodynamic behavior of the fully developed flow of conducting fluid," *Energies (Basel)*, vol. 14, no. 9, p. 2463, Apr. 2021.

[6] P. Haloi and T. K. Gogoi, "Performance assessment of a magnetohydrodynamic power generation system: Division of the exergy destruction rate into its sub-portions," *Journal of Energy Systems*, vol. 6, no. 2, 2022.

[7] D. Culver and Y. Urzhumov, "Forced underwater laminar flows with active magnetohydrodynamic metamaterials," *Phys Rev E*, vol. 96, no. 6, 2017.

[8] N. A. Zainal, R. Nazar, K. Naganthran, and I. Pop, "Unsteady MHD mixed convection flow in hybrid nanofluid at three-dimensional stagnation point," *Mathematics*, vol. 9, no. 5, 2021.

[9] O. M. Al-Habahbeh, M. Al-Saqqa, M. Safi, and T. A. Khater, "Review of magnetohydrodynamic pump applications," *Alexandria Engineering Journa*l, vol. 55, no. 2. 2016.

[10] W. Yang, Q. Jiu, and J. Wu, "The 3D incompressible magnetohydrodynamic equations with fractional partial dissipation," *J Differ Equ*, vol. 266, no. 1, 2019.

[11] E. R. Priest and T. G. Forbes, "The astronomy and astrophysics the magnetic nature of solar flares," *Astronomy and Astrophysics Review*, vol. 10, 2002.

[12] J. N. J. Mohamed, V. Rathinasamy, K. Karuppan, and R. Parthasarathy, "Numerical investigation of convective cooling in a rectangular vented cavity with two inlets and a hot obstacle," *Numeri Heat Transf A Appl.*, vol. 2, 2022.

[13] M. Shanmugapriya, "Magnetohydrodynamic (MHD) mixed convective flow and heat transfer over an inclined plate with radiation effect," *ARPN Journal of Engineering and Applied Science*s, vol. 11, no. 3, 2016.

[14] M. S. Hossain, Md. M. Hoque, and M. M. Kamruzzaman, "Effects of conduction on magneto-hydrodynamics mixed convection flow in triangular enclosures," *Mathematical Theory and Modeling*, vol. 3, pp. 49–67, 2013.

[15] S. Parvin and N. F. Hossain, "Investigation on the conjugate effect of Joule heating and magnetic field on combined convection in a Lid driven cavity with undulated bottom surface," *J Advan Sci Eng Res.*, vol. 1, pp. 210–223, 2011.

[16] S. Kherroubi, K. Ragui, N. Labsi, Y. K. Benkahla, and A. Boutra, "Three-dimensional numerical study of mixed convection within a ventilated cavity (Shape 'L') crossed by a nanofluid under the effect of a magnetic field," *MATEC Web of Conferences*, vol. 307, 2020.

[17] S. H. Hussain and Q. R. A. Amer, "Mixed convection heat transfer flowof air inside a sinusoidal corrugated cavity with a heat-conducting," *Journal of Enhanced Heat Transfer*, vol. 18, no. 5, 2011.

[18] M. Rahman, M. A. Alim, S. Saha, and M. K. Chowdhury, "Mixed convection in a vented square cavity with a heat conducting horizontal solid circular cylinder," *Journal of Naval Architecture and Marine Engineering*, vol. 5, no. 2, 2009.

[19] M. F. Alam, M. K. Bora, B. Sharma, and R. N. Barman, "Numerical investigation of magneto-hydrodynamics mixed convection in a square cavity for various shaped conducting obstacles placed at the center," *Mathematical Modelling of Engineering Problems*, vol. 6, no. 4, 2019.

[20] W. Hassen *et al.* (2021). Control of Magnetohydrodynamic Mixed Convection and Entropy Generation in a Porous Cavity by Using Double Rotating Cylinders and Curved Partition. ACS Omega. [Online]. Available: https://doi.org/10.1021/acsomega.1c05334

[21] M. R. Kazi, M. M. Ali, M. Hakim, and M. Rahman, "Magnetic mixed convection in a vented cavity with volumetric heat generation or absorption in presence of a cylindrical obstacle," *International Journalof Thermofluid Science and Technology*, vol. 8, no. 3, 2021.

[22] M. M. Ali, "Magnetohydrodynamic mixed convection in a nanofluid filled tubular enclosure," *Fluid Mechanics research International Journal*, vol. 4, no. 1, 2020.

[23] M. M. Rahman, M. A. H. Mamun, R. Saidur, and S. Nagata, "Effect of a heat conducting horizontal circular cylinder on MHD mixed convection in a lid-driven cavity along with joule heating," *International Journal of Mechanical and Materials Engineerin*g, vol. 4, no. 3, 2009.

[24] G. Tang *et al.* (2021). Numerical simulation of mixed convection in a two-sided lid-driven square cavity with four inner cylinders based on diamond arrays. *International Journal of Modern Physics C*. [Online]. Available: https://doi.org/10.1142/S0129183121500091

[25] M. U. Ahammad, M. M. Rahman, and and M. L. Rahman, "Mixed convection flow and heat transfer behavior inside a vented enclosure in the presence of heat generating obstacle," *Int J Innov Appl Stud*, vol. 3, no. 4, 2013.

[26] A. I. Rais, *et al.* (2023). Influence of heat generation/absorption on mixed convective flow in a lid-driven chamber with isothermal rotating cylinder. [Online]. Available: https://doi.org/10.1016/j.anucene.2022.109596

[27] M. M. Ali, R. Akhter, M. A. Alim, and M. M. Miah, "Magnetic-mixed convection in nanofluid-filled cavity containing baffles and rotating hollow-cylinders with roughness components," *Math Probl Eng.*, vol. 202, 2022.
[28] R. A. Mahmood *et al.* "Natural convection from a horizontal cylinder placed in a square enclosure: CFD simulations," *AIP Conference Proceedin*gs, vol. 2830, no. 1, 2023.
[29] M. M. Ali, S. Rushd, R. Akhter, and M. A. Alim, "Magneto-hydrodynamic mixed convective heat transfer in a nanofluid filled wavy conduit having rotating cylinders," *Scientia Iranica*, vol. 29, no. 2, 2022.
[30] K. M. Shirvan, M. Mamourian, S. Mirzakhanlari, and M. Moghiman, "Investigation on effect of magnetic field on mixed convection heat transfer in a ventilated square cavity," *Procedia Engineering*, vol. 3, 2015.
[31] M. M. Ali, M. A. Alim, and S. S. Ahmed, "Magnetohydrodynamic mixed convection flow in a hexagonal enclosure," *Procedia Engineering*, vol. 4, 2017.
[32] B. Gunnar, "Fields of physics by finite element analysis using flexpde," by GB Publishing and Gunnar Backstrom Malmo, Sweden, 2005.
[33] H. P. Langtangen, K. A. Mardal, and R. Winther, "Numerical methods for incompressible viscous flow," *Adv Water Resour*, vol. 25, no. 8–12, 2002.
[34] R. Y. Farsani, B. Ghasemi, "Magnetohydrodynamic mixed convective flow in a cavity," *International Journal of Mechanical and Mechatronics Engineer*ing, vol. 5, no. 11, pp. 2328–2331, 2011.
[35] D. B. Ingham and I. Pop, *Transport Phenomena in Porous Media III*, Elsevier Science, 2005.
[36] M. M. Hossain and M. A. H. Khan, "Stability of MHD wall driven flow through a tube," in *Procedia Engineering*, vol. 2, 2017.